Soft Matter

Cite this: *Soft Matter*, 2012, **8**, 5765

www.rsc.org/softmatter

PAPER

A three dimensional soft matter cell model for mechanotransduction

Xiaowei Zeng[b] **and Shaofan Li***[a]

Received 9th November 2011, Accepted 15th March 2012
DOI: 10.1039/c2sm07138j

An active multiscale three-dimensional (3D) soft matter cell model is developed to study the mechanotransduction of stem cells in an attempt to explain mechanical information exchange between the cells and their extracellular environment. In the proposed soft matter cell model, the cortical actin–myosin flow or the cytoplasmic flow is modeled as an active nematic fluid gel, the cell nucleus is modeled as a hyperelastic medium, and the ligand–receptor interaction between the cell and extracellular matrix is modeled by a coarse-grained molecular adhesive potential. We have implemented the soft matter cell model in a Lagrange type meshfree Galerkin formulation, and we have developed computational algorithms for adhesive contact between the cell and substrate. A comparison study with experimental data has been conducted to validate the parameters of the cell model. By using the soft matter cell model, we have simulated soft adhesive contact/spreading process between the cell and the extracellular substrate. The numerical simulation shows that the cell can sense substrate elasticity in a variety of different ways from cell spreading motion to cell shape and configuration changes.

1. Introduction

The ability of the cell to sense environmental mechanical stimulus and subsequently to mediate its own coordinated responses is called mechanotransduction.[1,2,3] As a cellular signal transduction process in response to mechanical stimuli, mechanotransduction plays important role in normal physiological processes such as cell motility, angiogenesis, embryonic development, tissue regeneration, and wound healing. However, abnormal mechanotransduction is also responsible for a series of diseases in cardiology, orthopedics, neurology, and oncology. The exact molecular mechanism for mechanotransduction of focal adhesion is still unknown, and it is under active investigation. Recent studies have connected the effect of mechanotransduction to the mechanism of stem cell differentiation, *e.g.* ref. 4 and 5. It has been found that behaviors of stem cells at early stage depend sensitively on both the rigidity as well as surface micro-structures of the extracellular environment, and that matrix elasticity directs stem cell lineage specification.

When cultured onto artificial adhesive surfaces, cell first flatten and deform extensively as they spread.[6] The early effect of the mechanotransduction due to cell contact and adhesion is translated into cortical motion,[7] which will then be reflected by the cell spreading speed, area, and morphology. Because this process is a mechanical interaction between the cell and the extracellular matrix (ECM), it strongly depends on the stiffness of ECM and other mechanical properties of the ECM. Not all cells of different types respond to elastic stiffness of the substrate in the same way, but many including endothelia cells,[8] mammary epithelial cells,[9] and mesenchymal stem cells,[5] exhibit increased spreading and adhesion on stiffer substrates compared to softer ones.[10]

In recent years, several cell mechanotransduction and rigidity sensing models have been proposed:

- Continuum elasticity model;[11]
- One-dimensional cluster model;[12]
- Contractility/Adhesion cooperation model;[13]
- Thermodynamic self-assembly model;[14]
- Force regulation model;[15]
- Crosstalk model;[16]
- Shear-lag model;[17]
- Force-induced adsorption model;[18]
- Two-spring rigidity sensing model;[19]
- Cell dipole model;[20]
- Pre-stress cell model;[21]
- Actomyosin contractility model;[22]
- Non-linear elasticity of ECM/Cell interaction model;[10]
- Stress-fibre polarization model.[23]
- A mechano-sensing and force generation model in contractile cells.[24]

These are very successful models with biology insights, however most of these models are one-dimensional or two-dimensional elasticity models. Three dimensional models are scarce, even the author of the two-spring model[19] conceded that 'a three-dimensional elasticity analysis as well as other features of cell mechanics should be included'. The contributors of these cell elasticity theories are from diverse fields: physics or bio-physics, bio-engineering, materials science, chemistry or bio-chemistry, and applied mechanics. At the same time, several general cell

[a]*Department of Civil and Environmental Engineering, University of California, Berkeley, CA 94720, USA. E-mail: shaofan@berkeley.edu*
[b]*Department of Mechanical Engineering, University of Texas, San Antonio, TX 78249, USA*

contact and focal adhesion models have also been proposed, *e.g.* ref. 25. Continuum models have been recently developed to study cell adhesion in the early stage,[26,27] and to simulate cell crawling.[28] An analytical model has been proposed to study kinetics of cell membrane spreading.[29,30]

The main novelty and distinction of the present work is using an active soft matter model to probe mechanotransduction of stem cells. Even from a mechanical perspective, a cell is not simply an elastic or viscoelastic medium. A large component of cells is cytoplasm, which is a thick liquid gel residing between cell membrane and cell nucleus. The cytoplasm contains abundant actin proteins, and they are responsible for transmitting force and other mechanical signaling, and forming stress fibers. It is generally accepted that the force transmission process in cells is through a two-headed binding process of a successive myosin to F-actin inter-connection. Even though the molecular mechanism of this event has been known for years, how aggregated actin filament network comes together, how to predict the overall behavior of actin-network dynamics, and how it is related to cell motion, are still open questions. Various actin–myosin dynamics models have been proposed in the literature, *e.g.* viscoelastic flow model.[31] All these models recognize the fact that the myosin-generated viscoelastic actin flow may provide important clues to cell motility, migration, cell shape change, division, formation of focal adhesion, and mechanotransduction.

It was known since the early 1990s that F-actin may undergo an isotropic-to-nematic liquid crystalline phase transformation when the actin network concentration reached a certain level. In other words, above a threshold of protein concentration, F-actin solutions may form a phase of nematic liquid crystal or undergo isotropic to nematic phase transition.[32–35] This physiological event has been thoroughly investigated in the past decade *e.g.* ref. 36–38. *In vivo* conditions, the aggregate of actin network inside a cell behaves somewhat like a nematic liquid crystal gel, which is one of defining properties of cell cytoplasm at mesoscale level.

Actin in cells is found both in a globular monomer state (G-actin) and in a filament state (F-actin). It is constantly interchanging between these two states from time to time and from location to location, which is the essential feature of actin–myosin dynamics. On the other hand, viscoelasticity—the traditional focus of cell mechanics—is only one facet of a complex, biological, thermodynamic system. The present work hopes to establish a computational soft matter model that can reveal some of fundamental characteristics of cytosekelton/cytoplasm dynamics and hence the overall effects of mechano-transduction of actin network in the cell. In Fig. 1, we compare the micro-structure of actin–myosin filaments with that of nematic liquid crystals, specifically in the spatial mesogen

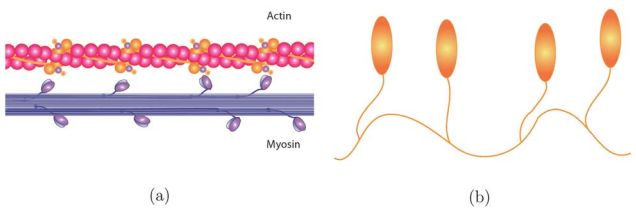

Fig. 1 (A) Microstructure of actin–myosin filaments and (B) micro-structure of the mesogen of nematic liquid crystal.

structure, readers may find the similarity and affinity of the two. Therefore, at the mesoscale level, a nematic liquid crystal gel is a suitable bio-physical model for both plasma membranes and cytoplasm.

In order to understand the precise mechanical cellular sensing mechanism during cell contact and adhesion and to explain the detailed mechanotransduction process of the event, we have developed an active multiscale soft matter cell model for simulation of cellular mechanotransduction process. In a recent paper,[39] we reported some early results of this study. The main difference between this paper and ref. 39 is that the numerical calculations presented here are based on a full three-dimensional modeling and simulation of an active soft matter cell model, whereas the simulation results presented in ref. 39 are two-dimensional simulations of a passive cell model.

2. Mesoscale continuum modeling of cell and ECM

To model a biological cell using today's computational resources and technology, mesoscale continuum modeling is still the best approach. This is because mesoscale modeling has distinct advantages by providing the most direct and relevant information on the bio-physical and physiological state of the cell.

The most successful cell (membrane) model today is still the fluid mosaic model—the lipid bilayer model.[40] A popular mechanics model that is associated with the fluid mosaic model is Helfrich's liquid crystal membrane model,[41] which takes into account the crystalline structure of lipid bilayers. Because of its biological relevance, it has been widely used in modeling plasma membranes at the mesoscale.

For a long time, the modeling of cytoskeleton medium has been mainly based on linear elastic, or hyper-elastic models, *e.g.* ref. 42. It was not until recently that a three-dimensional visco-elastic cell model,[43] mixture model,[24] and complex fluid model on retrograde flow and lamellipodium motion[58] started to appear in the literature.

It has been argued by many researchers that the homogeneous elastic or viscoelastic continuum cell model cannot predict long-distance mechanotransduction *e.g.* ref. 21. According to the fundamental (Boussinesq) solution of linear elasticity, the stress response at a spatial point to a point load is proportional to inverse square distance between the point of loading and the location where stress is measured, *i.e.* $\sigma \sim 1/R^2$. This elastic contact stress characterization prohibits long-distance stress sensing. Laboratory measurements found that the stress field in cells due to a mechanical load is 10 times stronger than the elastic solution predicts. To achieve an agreement with bio-physical or physiological reality, some have introduced pre-stress cell models such as the tensegrity cell model *e.g.* ref. 44 and 45. In it the contact stress characterization is proportional to the inverse distance of the two points, *e.g.* $\sigma \sim 1/R$, so that long distance sensing is possible. The current trend of continuum cell modeling is to develop a continuum level actin-network fluid dynamics that addresses myosin–actin interaction and dynamics directly at the mesoscale, *e.g.* ref. 31 and 46

The main objective of this work is to advance mesoscale modeling of cellular processes, in particular mechano-transduction of stem cells, by developing an active soft matter cell model that can synergistically combine the main features and

essential elements of different continuum cell models into one single model, such as predicting pre-stress state, describing actin–myosin dynamics, reflecting complex nature of the non-Newtonian viscoelastic fluid, and capturing the cell motility and contractile motions, *etc.*

To accomplish this goal, we propose a soft matter continuum model for mechanotransduction of cells and the related computational framework. The multi-component cell model proposed here consists of several elements: an active nematic gel medium, a hyperelastic or visco-hyperelastic nucleus, and a small scale adhesive field that is used to mimic the ligand–receptor interaction. The multiscale two-layer soft matter cell model is illustrated in Fig. 2.

It is well known that the cell plasma membrane is described as being a fluid because of its hydrophobic integral components such as lipids and membrane proteins that move laterally or sideways throughout the membrane without encountering much resistance.[40] Therefore, the cell membrane may be effectively modeled as a liquid crystal membrane *e.g.* ref. 41. On the other hand, a detailed examination of the cell cytoplasm reveals similar characteristics: cell cytoplasm does not only consist of liquid, but also contains cell organelles and many weakly cross-linked polymer networks, such as actin filaments or intermediate filaments. Therefore an aggregate of undeveloped stem cell interior may be approximated as a complex fluid with organelles, filaments, and proteins. Depending on the phenotype, the content, *i.e.*, microstructure and the concentration, of these filaments may be different. In this work, we are only interested in modeling stem cells. For embryonic stem cells, their cellular structure is still under development, some of the complexity in cellular structure may be simplified. According to ref. 47 the embryonic stem cells are ~10 fold softer than their differentiated counterparts. Therefore, the cytoplasm region of the stem cell may contain less polymer-form cytoskeleton but more liquid-form cytoplasm. Hence, a nematic liquid crystal gel model may be a suitable description for modeling a cytoplasmic actin aggregate. In the following section, we shall first discuss the proposed active liquid crystal gel model.

2.1. Active nematic hydrodynamics for cytoskeletal filaments

Liquid crystals have biphasic properties by exhibiting both liquid and solid characteristics. For instance, a liquid crystal may be fluid similar to a liquid with vanishing shear modulus, while having a long range orientational order and therefore a strain gradient elasticity associated with deformations of the order parameter. Many biological materials contain liquid crystalline phase, and the most common examples are cell membranes, phospholipids, cholesterol, DNA, and various proteins, among others.[48]

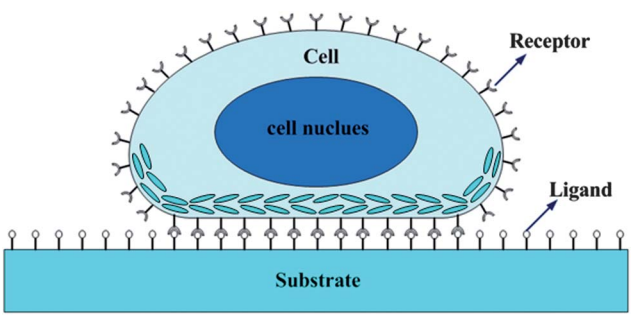

Fig. 2 Soft matter cell model.

Actin cytoskeleton filaments have polarity, and actin monomers orient with their cleft towards the pointed (or minus) end and their head towards to the barbed (or plus) end. Under suitable physiological conditions, G-actin monomers may be transformed to F-actin (polymer form) by ATP at the plus end, which is polymerization, and it may be depolymerized at the minus end. For mesoscale modeling, we may assign a unit vector at each material point, hence a continuous director field may be established to represent local polarization of a homogenized actin filament/cytoplasm representative volume element (RVE). This is the bio-physical foundation or justification for developing nematic gel hydrodynamics to model a polar actin filament/cytoplasm gel at the mesoscale level. The local orientation of this director field is central to many cellular processes such as cell motility and locomotion, cell adhesion, and cell division.

Although the liquid crystal behavior of cytoskeletal filaments were discovered in early 1990s, it is not until recently that people have started to model actin cytoskeleton motion or lamellipodium motion by using nematic liquid crystal hydrodynamics.[58–61] In fact the cell is a living object, so the conventional passive liquid crystal hydrodynamics is insufficient to model many important features of a living cell. This is because the free-energy based soft matter approach may not be valid, because it is intended for systems at equilibrium states.

In eukaryotic cells, actomyosin filaments are networks of viscoelastic gels interacting with myosin molecular motors driven by hydrolysis of adenosine triphosphate (ATP), which is an active biological polar gel. Several hydrodynamics theories of active polar gels, or active nematic gels, have been developed for the cytoskeleton or cytoskeleton/cytoplasm aggregates *e.g.* ref. 56, 57 and 61–63.

For simplicity, in this work we propose a simplified active-filament hydrodynamics that combines a simplified version of the Ericksen–Leslie theory for nematic gels[49] with an additional active stress term (see ref. 64). Note that in this paper, we mainly use standard indicial notation. To capture large deformation and motility of the cell, we adopt a Lagrangian approach, which involves tensorial quantities defined in different configurations. We distinguish the Euclidean triad of the unit vector basis in spatial configuration by using $\mathbf{e}_i, i = 1,2,3$ and that in referential configuration, by using $\mathbf{E}_I, I = 1,2,3$.[71] Based on that convention, the strong forms of the equation of motion and the modified hydrodynamics equation for the active nematic gel are as follows,

$$\rho \frac{\mathrm{D}v_i}{\mathrm{D}t} = \sigma_{ji,j} + b_i, \ \forall \mathbf{x} \in \Omega(t) \tag{1}$$

$$\rho^{\mathrm{d}} \frac{\mathrm{D}\tilde{h}_i}{\mathrm{D}t} = \gamma \left\{ h_{i,jj} - r_i(\mathbf{h}) \right\}, \ \forall \mathbf{x} \in \Omega(t) \tag{2}$$

where $\mathbf{v} = v_i \mathbf{e}_i$ is the velocity field, $\mathbf{h} = h_i \mathbf{e}_i$ denotes the nematic director field, $\mathbf{b} = b_i \mathbf{e}_i$ is the body force in the current configuration, and $\mathbf{e}_i, i = 1,2,3$ are triad of unit basis vectors for spatial coordinate. ρ and ρ^{d} are densities for fluid and director fields in the current configuration respectively. Note that the differential gradient operator is defined in the spatial

configuration, *i.e.* $\nabla := \frac{\partial}{\partial x_i}\mathbf{e}_i$; γ is the director elastic constant, $\mathbf{r}$ is a Landau–Ginzburg type potential that enforces the unit vector condition for the director field,

$$r_i = \frac{\mathrm{d}R(\mathbf{h})}{\mathrm{d}h_i} = \frac{h_i}{\epsilon^2}\left(|\mathbf{h}|^2 - 1\right), \quad \text{and} \quad R(\mathbf{h}) = \frac{1}{4\epsilon^2}\left(|\mathbf{h}|^2 - 1\right)^2 \tag{3}$$

and the Cauchy stress is determined as

$$\sigma_{ij} = -p\delta_{ij} + 2\mu d_{ij} - \eta h_{k,i}\, h_{k,j} - \zeta h_i h_j \tag{4}$$

In eqn (4), p is the hydrostatic pressure, μ is viscosity, η is a positive constant. It should noted that in eqn (2), $\frac{\mathrm{D}\tilde{\mathbf{h}}}{\mathrm{D}t}$ denotes the objective rate, which is very important in nonlinear large deformation simulation. To the best of the authors' knowledge, this point has been often neglected in many complex fluid mechanics literatures. In our computations, $\frac{\mathrm{D}\tilde{\mathbf{h}}}{\mathrm{D}t}$ is the objective rate, and it is chosen as

1. The convected rate: $\overset{\circ}{h}_i = \frac{\mathrm{D}h_i}{\mathrm{D}t} + \ell_{ki}h_{kj}$;

or

2. The corotational rate: $\overset{\triangle}{h}_i = \frac{\mathrm{D}h_i}{\mathrm{D}t} - w_{ik}h_{kj}$;

and ℓ is the velocity gradient, and $\mathbf{w}$ is the spin tensor,

$$\ell_{ij} = \dot{F}_{iK}F^{-1}_{Kj}, \text{and } w_{ij} = \frac{1}{2}\left(\ell_{ij} - \ell_{ji}\right)$$

The last term in eqn (4), $\zeta h_i h_j$, is the active stress term adopted (see ref. 64). This active stress term represents the dipolar force generated by the director field, which may not be able to derive from a standard free energy approach. This dipolar stress field is believed to be the element for a host of cellular activities including cell motility, mechanotransduction, and some other aspects of actin flows.[20] To achieve the contractile effect, we choose $\zeta = -0.001$ in this paper. That choice of coupling constant produces a smaller active stress than the real contractile stress in cells. By using a realistic contractile stress coefficient, interesting cellular behavior will become available, such as cell motility. However, we have found that additional simulation techniques may be needed in order to assure the numerical stability of the computation, because in this case additional energy is being added into the cellular system. This part of the work is in progress. In fact, even with a presence of small contractile stress, the cell may start to move (see Fig. 12). A systematic modeling and simulation of three-dimensional cellular contractile motion and cell motility will be reported in a different paper.

To test the viscoelastic property of the active nematic gel model, we designed a 1D bar problem (length $L = 1.0 \times 10^{-4}$ m). A unit director is assigned at both ends, with initial directions of $\pi/6$ and $\pi/3$, respectively. The left end is fixed and a sine displacement is prescribed at the right end as $u = U_{\max}\sin(2\pi ft)$, where $U_{\max} = 0.25 \times 10^{-4}$ m. At different frequencies for a complete cycle, we obtained different loops (see Fig. 3). As the frequencies decrease from $f = 1.0 \times 10^5$ s^{-1}, the loop eventually becomes a straight line.

2.2. Hyperelastic model

The cell nucleus plays a central role in cellular response to mechanical forces.[50] According to ref. 51 the nucleus inside the cell is about 9 times stiffer than the cytoplasm. Based on these observations, we model the cell nucleus as a hyperelastic material, which has been used in ref. 50 to model the nucleus of endothelia cells.

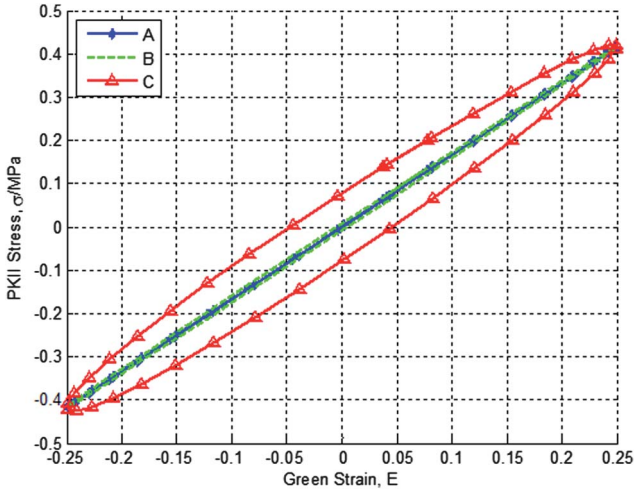

Fig. 3 Hysteresis loop from the Nematic gel model ($\zeta = 0.0001$): A: $f = 1.0 \times 10^3$, B: $f = 1.0 \times 10^5$, C: $f = 1.0 \times 10^6$.

There are more than 20 hyperelastic models for rubber-like materials in the literature, a comparison of different hyperelastic models can be found in ref. 52. In this research, we adopted the modified Mooney–Rivlin material[53] to model the cell nucleus. The strain energy density function W for the modified Mooney–Rivlin material is given as follows,

$$W = C_1\left(I_1 - 3I_3^{1/3}\right) + C_2\left(I_2 - 3I_3^{2/3}\right) + \frac{1}{2}\lambda(\ln I_3)^2 \tag{5}$$

where C_1,C_2 and λ are material constants; $\mathbf{C} = \mathbf{F}^{\mathrm{T}}\cdot\mathbf{F}$ is the right Cauchy–Green deformation tensor, and its three invariants are defined as

$$I_1 = C_{II},\ I_2 = \frac{1}{2}[C_{II}C_{JJ} - C_{IJ}C_{JI}],\ I_3 = \det(C_{IJ}) \tag{6}$$

The corresponding constitutive relations can be expressed in terms of the second Piola–Kirchhoff stress tensor $\mathbf{S} = S_{IJ}\mathbf{E}_I \otimes \mathbf{E}_J$, and the invariants of the right Cauchy–Green tensor,

$$S_{IJ} = 2\{(C_1 + C_2I_1)\delta_{IJ} - C_2C_{IJ} - (C_1I_3^{1/3} + 2C_2I_3^{2/3} - \lambda lnI_3)C^{-}_{IJ}\} \tag{7}$$

After the second Piola–Kirchhoff stress is obtained, the first Piola–Kirchhoff stress tensor can be immediately computed as $\mathbf{P} = P_{iJ}\,\mathbf{e}_i \otimes \mathbf{E}_J = \mathbf{F}\cdot\mathbf{S} = F_{iK}\,S_{KJ}\,\mathbf{e}_i \otimes \mathbf{E}_J$, which can then be substituted into the later developed meshfree Galerkin formulation to calculate the internal nodal force.

2.3. Visco-hyperelastic model

The key to simulate cell spreading over the substrate is to capture the interaction between cells and their extracellular matrix (ECM). Fig. 2 illustrates a soft matter model for a cell/substrate system. The mechanical properties of extracellular matrix is often comparable with that of soft gels.[54,55] However, so far most continuum level ECM models still adopt the hyperelastic model.

One of the drawbacks of the hyperelastic model is its inability to describe energy dissipation during cell spreading. To take this into consideration, we model the extracellular matrix as a substrate of visco-hyperelastic block.

In the viscoelastic cell model, the stress contribution has two parts: the visco-stress part and the hyperelastic part, and the total Cauchy stress may be written as,

$$\sigma_{ij} = \sigma^{\mathrm{v}}_{ij} + \sigma^{\mathrm{h}}_{ij}$$

where $\boldsymbol{\sigma}^{\mathrm{h}}$ stands for the stress contribution from the hypereleastic part, and $\boldsymbol{\sigma}^{\mathrm{v}}$ represents the viscous stress. For the hyperelastic part,

$$\sigma^{\mathrm{h}}_{ij} = \frac{1}{J} F_{iK} S_{KL} \cdot F_{jL}$$

where J is the determinant of the deformation gradient, and the second Piola–Kirchhoff stress $\mathbf{S} = S_{IJ}\,\mathbf{E}_I \otimes \mathbf{E}_J$ is determined by eqn (7).

For the viscous part, we adopt the following formula proposed by Yang *et al.*[65,66] for rubber materials or elastomers. The Cauchy stress may be written as,

$$\sigma^{\mathrm{v}}_{ij} = F_{iK}(t)\left\{\int_0^t \left[A_1 + A_2(I_3 - 3)\right]\exp\left(-\frac{t-\tau}{A_3}\right)\dot{E}_{KL}(\tau)d\tau\right\}F_{jL}(t) \tag{8}$$

where A_1, A_2 and A_3 are three material parameters. Together with the modified Mooney–Rivlin material, we have six material constants, namely C_1, C_2, λ, A_1, A_2 and A_3. In simulations presented in this work, we choose

$$A_1 = 0.350 \times 10^7 \text{ Pa},\ A_2 = 0.830 \times 10^6 \text{ Pa},\ A_3 = 0.50 \times 10^{-5} \text{ s}.$$

3. Meshfree Galerkin formulation and simulation algorithm

One of the main objectives of this work is to develop a three-dimensional computational soft matter cell model that can be used in predictive simulations of realistic cellular motions. In this section, we briefly discuss the computational formulations that are used in simulations of cell deformation based on the continuum model eqn (1)–(4). The numerical simulations are conducted by using meshfree methods.[67] This is because that the meshfree method has some advantages in computing large deformation problems compared with traditional finite element method or finite difference method. In our meshfree simulation, both the cell and its substrate is discretized by a set of particles, and then we can build a meshfree shape function at each particle to form a continuous global interpolation field.

In order to simulate cell spreading over the substrate under extremely large deformation, a total Lagrangian meshfree formulation is developed for the soft matter cell model under finite deformation, and a related Galerkin weak formulation is derived and used in the numerical computation. The main advantage of adopting a meshfree Lagrangian formulation in simulation is its ability to avoid remeshing and easy-tracking of cell surface and interface. Consequently the corresponding simulation results are insensitive to mesh-distortion during cell spreading, whereas mesh-based finite element methods have difficulties handling such large deformations.

Starting from the strong form of the balance of linear momentum, eqn (1), and following the standard variational procedures *e.g.* ref 68 and 69, the variational Galerkin weak formulation of the balance of linear momentum under finite deformation can be derived by integration by parts from the weighted residual form,

$$\begin{aligned}\sum_{\alpha=1}^{2}\int_{\Omega_0^{(\alpha)}} \rho_0^{(\alpha)} \ddot{u}_i^{(\alpha)} \cdot \delta u_i^{(\alpha)} d\Omega_0^{(\alpha)} + \sum_{\alpha=1}^{2}\int_{\Omega_0^{(\alpha)}} P_{iJ}^{(\alpha)} \delta F_{iJ}^{(\alpha)} d\Omega_0^{(\alpha)} \\ = \sum_{\alpha=1}^{2}\int_{\Omega_0^{(\alpha)}} J^{(\alpha)} b_i^{(\alpha)} \delta u_i^{(\alpha)} d\Omega_0^{(\alpha)} \\ + \sum_{\alpha=1}^{2}\int_{\Gamma_{t0}^{(\alpha)}} \overline{T}_i^{(\alpha)} \delta u_i^{(\alpha)} dS^{(\alpha)} + \sum_{\alpha=1}^{2} \delta\Pi_{AC}^{(\alpha)}\end{aligned} \tag{9}$$

where $\delta u_i^{(\alpha)}$ are virtual displacement fields, $\delta F_{iJ}^{(\alpha)}$ is the variation of deformation gradient, $\mathbf{P} = P_{iJ}\,\mathbf{e}_i \otimes \mathbf{E}_J$ is the first Piola–Kirchhoff stress tensor, and $\bar{\mathbf{T}}$ is the prescribed traction on the traction boundary $\Gamma_t^{(\alpha)}$. Note that here the superscript index, $\alpha = 1$ corresponds to the cell, and the superscript $\alpha = 2$ corresponds to the extracellular matrix substrate. The last term of eqn (9), $\delta\Pi_{AC}^{(\alpha)}$, denotes the virtual work contribution from adhesive contact (see ref. 39). Readers can find a detailed computational algorithm for cell contact and adhesion in ref. 70.

Since the hydrodynamic equation for the nematic director is described for the cell only, we omit the superscript, $\alpha = 1$ in the formulation. Similar to the derivation of the weak form of equation of motion, a Galerkin variational weak formulation for hydrodynamics equation of nematic gel, eqn (2), can be obtained as follows,

$$\begin{aligned}\int_{\Omega_0} \rho_0^d \frac{\mathrm{D}h_i}{\mathrm{D}t}\delta h_i d\Omega_0 \ = \ -\int_{\Omega_0} \gamma J F_{Ij}^{-1} F_{Kj}^{-1} h_{\ell,I}\delta h_{\ell,K} d\Omega_0 \\ -\int_{\Omega_0} \gamma J r_i(\mathbf{h})\delta h_i d\Omega_0\end{aligned} \tag{10}$$

where $J = \det\mathbf{F}$, and we assume that on contact-free boundary Γ_{t},

$$N_I J F_{Ij}^{-1} F_{Jj}^{-1} h_{k,J} = 0, \forall \mathbf{x} \in \Gamma_{\mathrm{t}}$$

and on adhesive contact boundary,

$$h_i = \bar{h}_i \Rightarrow \delta h_i = 0, \forall \mathbf{x} \in \Gamma_c$$

where $\mathbf{N} = N_I\mathbf{E}_I$ is the out-normal of boundary surface in the referential configuration.

4. Coarse-grained adhesive contact model for cell-substrate interaction

Cell adhesion and motility are essentially dynamic interactions between cells and ECM substrates. The van der Waals force and repulsive steric force may provide a long range molecular interaction, which is usually referred to as nonspecific binding. During most cell adhesion, a strong covalent bond force is present at surface interaction site between ligands and receptors, which is termed as the specific binding.[77,78] In the following, we outline a coarse-grain adhesive contact model that is used in this work to simulate adhesive contact between the cell and the substrate.

The part of the virtual work contribution due to adhesive contact forces exerting on the body of the cell has two parts: (1) From the non-specific von der Waals force, and (2) From the specific ligand–receptor interaction,

$$\delta\Pi_{AC} = \int_{\Omega} b_i(\boldsymbol{\Delta})\delta u_i d\Omega + \int_{\Gamma_c} f_i \cdot \delta g_i dS \tag{11}$$

where the vector $\mathbf{g} = g_i\mathbf{e}_i$ is the position gap vector between two particles that are in the surface of the cell and the surface of the substrate.

In this work, the non-specific adhesive force (van der Waals) is modeled as an exponential type of forces,

$$b_i(\boldsymbol{\Delta}) = G\,\exp(-|\boldsymbol{\Delta}|/d_0)\,\frac{\Delta_i}{|\boldsymbol{\Delta}|}. \tag{12}$$

where $G = 100$ N Kg^{-1} (scaled) $\sim 10^6$ N Kg^{-1} (unscaled), and $d_0 = 1.0 \times 10^{-5}$ m are constants, and $\boldsymbol{\Delta} = \Delta_i\mathbf{e}_i$ is the distance position vector between nodal particles in the cell and the corresponding surface element of the substrate. The specific ligand–receptor bonding force, $\mathbf{f} = f_i\mathbf{e}_i$, is modeled by using an adhesive potential, and the interaction area between ligands and receptors is modeled as an interactive zone, or a gap (<100 nm), that separates the cell and its substrate. The adhesive force distribution varies according to the gap distribution between the two surfaces. In the adhesive contact algorithm, we adopt an adhesive potential given in ref. 28 and 79 in modeling adhesive interactions between a cell and a rigid substrate to study cell crawling,

$$\Phi(r) = \sigma\left[\left(\frac{\varepsilon}{r}\right)^4 - 2\left(\frac{\varepsilon}{r}\right)^2\right] \tag{13}$$

where σ is the energy depth and r is the gap length at a specific location. The adhesive force vector can be calculated as:

$$F_i(r) = -\frac{\partial\Phi}{\partial r_i} = \phi'(r)\frac{r_i}{r} \tag{14}$$

where

$$\phi'(r) = \frac{4\sigma}{\varepsilon}\left\{\left(\frac{\varepsilon}{r}\right)^5 - \left(\frac{\varepsilon}{r}\right)^3\right\} \tag{15}$$

Taking ligand–receptor bond density into consideration, we can calculate adhesive force between the cell membrane and the substrate surface based on the following formula,

$$f_i(r) = N_{\mathrm{b}}F_i(r) = N_{\mathrm{b}}\frac{4\sigma}{\varepsilon}\left\{\left(\frac{\varepsilon}{r}\right)^5 - \left(\frac{\varepsilon}{r}\right)^3\right\}\frac{r_i}{r} \tag{16}$$

where N_{b} is the bond density. In our simulations, we choose $N_{\mathrm{b}} = 500$ μm^{-2} and $\sigma = 0.024$ pN μm based on the data parameter selection in ref. 28. In addition to above data selection, we choose $\varepsilon = 100$ nm, time step $t^* = 1.0 \times 10^{-10}$.

It may be noted that the interface condition between air and cell is also important in the cell spreading simulation. It is enforced by the following equation,

$$\sigma_{ij}n_j = -(\sigma_0\kappa + p_0)n_i, \forall\,\mathbf{x} \in \Gamma_{\mathrm{cell/air}}, \tag{17}$$

where σ_0 is the surface tension, and we choose $\sigma_0 = 0.072$ mN m^{-1}; p_0 is the ambient pressure, and we choose $p_0 = 100$ kPa. $\Gamma_{\mathrm{cell/air}}$ is the interface between the cell and atmosphere. The mean surface curvature for air/cell interface may be calculated as,

$$\kappa = \nabla_x \cdot \mathbf{n} = n_{i,i} = F^{-1}_{I,i}n_{i,I}$$

where $\mathbf{F} = F_{iJ}\mathbf{e}_i \otimes \mathbf{E}_J$ is the local deformation gradient.

5. Modelings and simulations

In this section, we present the modeling and simulation results of cell spreading, in which we apply the proposed soft matter cell model together with the coarse-grained contact-adhesion algorithm to study mechanotransduction of stem cells by simulating its contact and adhesion with an extracellular matrix. To ensure a meaningful simulation, we first conduct the model validation and verification tests. By doing so, we can identify the parameters of the soft matter cell model. Then we applied the verified cell model to simulate cell contact with substrates of different stiffness.

5.1. Model validation: Comparison with experimental data

To validate the proposed cell model, we have used the cell model to simulate cell deformation under compression and compared with experiment measurements obtained for endothelial cells.[50] The constant force is applied at the top and bottom of the rigid micro-plate, and the boundary nodes are in contact with the cell surface. In the simulation, the cell deformation is defined as the relative reduction in height, *i.e.* $(H_0 - H)/H_0$.

We have used a hyperelastic material to model stem cell nucleus, because it has been used and validated in modeling endothelial cell nucleus.[50] The region outside of the cell nucleus, *i.e.* the cytoskeleton/cytoplasm medium, is modeled as an active nematic liquid gel. To obtain the model parameters, we fit the force–deformation curve (see Fig. 4(c)) in determining the material constants.

Fig. 4(a) and (b) show cell shapes before and after deformation. The load-deflection curve is plotted in Fig. 4(c). The applied compressive force increases non-linearly as a function of the cell height reduction. From the simulation (see Fig. 4(c)), one can find that the force required to create the same deformation for endothelial cells is larger than that of stem cells. This is reasonable when one considers that the stem cells are undeveloped cells. According to ref. 47 the embryonic stem cells are ~10 fold softer than their differentiated counterparts. It can be seen from Fig. 4 that our stem cell model ($r = 0.382R$ and $r = 0.618R$) is much softer than endothelial cells, which is most likely true in reality.

5.2. 3D Cell spreading on different substrates

As reported in ref. 10, cell spreading over the substrate is a (substrate) stiffness-dependent process, *e.g.* the cell exhibits increased spreading and adhesion on stiffer substrates. Attempting to replicate the experimental observations, we first simulate cell spreading on substrates with different stiffness in three-dimensional space.

In the following simulations, the cell is modeled as a perfect 3D spherical ball initially in the referential configuration, with a diameter of $D = 10$ μm (see Fig. 5). The substrate is modeled as a 3D circular plate with a dimension of ($R \times H = 15$ μm $\times$ 5 μm). In the meshfree computation, a total of 4341 particles are used in discretization of the cell, and 16 640 particles are used in meshfree discretization of the substrate.

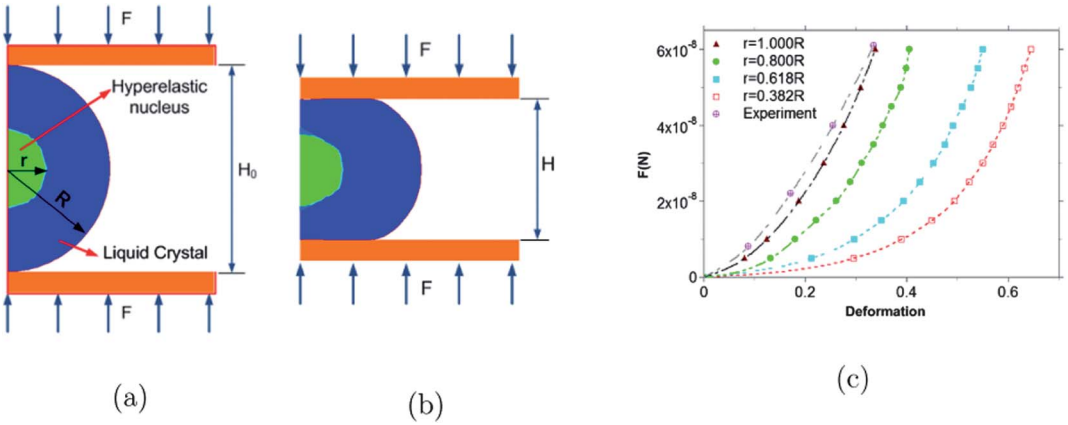

Fig. 4 Validation of the cell model: (a) Before deformation; (b) After deformation; (c) Force-displacement curve.

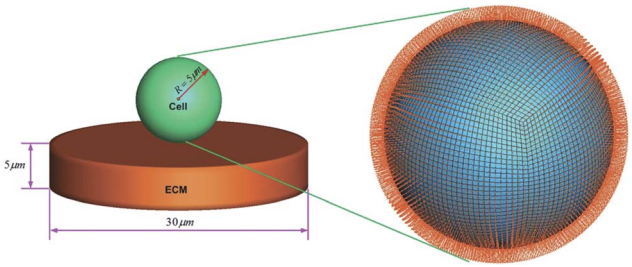

Fig. 5 A 3D Computational model.

In this study, the nucleus of the cell is modeled as a hyperelastic material of Mooney–Rivlin type. The initial density is $\rho^0 = 1.0 \times 10^3$ kg m^{-3}, and the material constants are $C_1^n = 2.126 \times 10^3$ Pa, $C_2^n = 1.700 \times 10^2$ Pa and $\lambda^n = 1.700 \times 10^5$ Pa. The region outside the hyperelastic nucleus is modeled as a nematic liquid gel.

The substrate is modeled as a visco-hyperelastic material described earlier. Three different substrates with different stiffness are considered. The density for three substrates are the same as that of the cell nucleus. We define the material constants $C_1 = 1.265 \times 10^4$ Pa, $C_2 = 1.012 \times 10^3$ Pa and $\lambda = 1.012 \times 10^6$ Pa. The material constants for three different substrates are chosen as,

$$C_1^{S1} = 2C_1,\ C_1^{S2} = 5C_1,\ C_1^{S3} = 10C_1$$

$$C_2^{S1} = 2C_2,\ C_2^{S2} = 5C_2,\ C_2^{S3} = 10C_2$$

$$\lambda^{s1} = 2\lambda,\ \lambda^{s2} = 5\lambda,\ \lambda^{s3} = 10\lambda$$

At the start of the simulation, the cell is kept still, and it is in a suspension state; we release the cell when the computation starts. The initial gap between the lowest point of the cell and substrate is set at 200 nm, and the bottom surface of the substrate is fixed during the entire simulation period.

In Fig. 6, we depict the effective stress contours on the surface of the deformed cell body on three substrates with different stiffness under the same contact conditions at the same time. As expected, one may find that the contact between the cell and softest substrate (substrate-I) (Fig. 6 (a)) generates the least cell spreading, and the contact between the cell and substrate-II (Fig. 6(b)) has the second least cell spreading, and the cell on the substrate-III generates the most spreading (Fig. 6(c)). After the stiffness of the substrate reaches a critical value, if one keeps increasing the substrate stiffness, the rate of spreading increase may become very small, or not sensitive to the substrate elasticity. This indicates that the cell spreading speed may reach a limit when the stiffness of the substrate reaches a certain critical value. However, within a certain range the cell spreading area is directly affected by elastic stiffness of the substrate, and such a correlation, we believe, is purely a bio-physical phenomenon of soft matter. From Fig. 7(a), one can clearly observe that as the substrate stiffness increases the spreading area increases.

Since the computation is done based on a mesoscale continuum model, one can measure the stress at every point of the cell. In Fig. 8, we depict the computed effective stress distribution on the surface of the deformed bodies of a same type of cells, which are in contact with three substrates of different elastic modulus (stiffness). We have found that the stress distribution in both the cell and the substrate are different if the substrate elasticity is different, which indicates that the cell can sense the substrate elasticity and response to it. The mechanical signals between the cell and substrate are transmitted through adhesive contact interaction between the cell and substrates. Furthermore, we have sampled the effective stress in the cell nucleus from different sets of cell/substrate computations at the beginning stage of the soft contact. At the same time, we compare the magnitudes of the effective stress *versus* those obtained from substrates of different stiffness, which is shown in Fig. 7(b). The effective stress is defined as:

$$\sigma_e = \frac{1}{\sqrt{2}}\left[(\sigma_1 - \sigma_2)^2 + (\sigma_2 - \sigma_3)^2 + (\sigma_3 - \sigma_1)^2\right]^{1/2} \quad (18)$$

From Fig. 7, one can clearly observe the fact that as the substrate stiffness increases the magnitude of the effective stress increases. A similar correlation has been observed in the experimental measurement of stem cell contractile force *e.g.* ref. 4. Fig. 9 displays a time sequence of a cell spreading over Substrate III. The color contour is the effective stress contour, and the white arrow represents the director field. Compared to 2D simulations, 3D simulations provide a possible way to capture the cell morphology changes described in ref. 73.

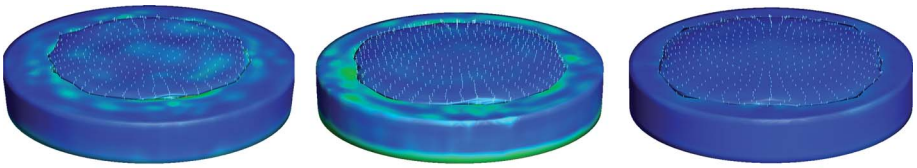

(a) (b) (c)

Fig. 6 Cell spreading over substrates with different stiffness: (a) Substrate-I, (b) Substrate-II, (c) Substrate-III.

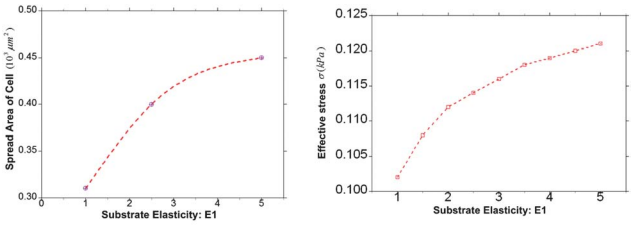

(a) (b)

Fig. 7 (a) Spreading area and (b) Effective stress *vs.* elastic stiffness of the substrate.

We would like to make note of an important point: it is essential, or almost necessary, to conduct a full three-dimensional computation for cell spreading simulation. In Fig. 10, we display a time sequence of a cell spreading over a deformable substrate, which was obtained in an axisymmetric computation. So it is essentially a two-dimensional simulation. One may find that the cell spreading morphology in this case is very much different from that obtained from a full 3D simulation, *e.g.* Fig. 9. It can be noted that in this particular axisymmetric simulation there is no active stress used in constitutive modeling of the cell. Other than that, and except some material constant differences, the computational formulations for both cases are almost identical. However, from Fig. 10, one cannot observe the rough and wavy cell spreading front that can be observed in Fig. 9.

5.3. Cell response in a stiffness-varying substrate

One of the advantages of the soft matter cell model proposed here is its potential to describe actomyosin dynamics and lamellipodium dynamics, which are the central issues of modeling cell motility and migration. It is therefore interesting to examine cell spreading on a substrate that has non-uniform stiffness, because the non-homogeneous external stimuli may trigger contractility responses of actomyosin dynamics inside the cell.

For this purpose, we consider an ECM substrate with varying elastic modulus along the circumferential direction, and we place a cell onto the substrate while observing the cell spreading

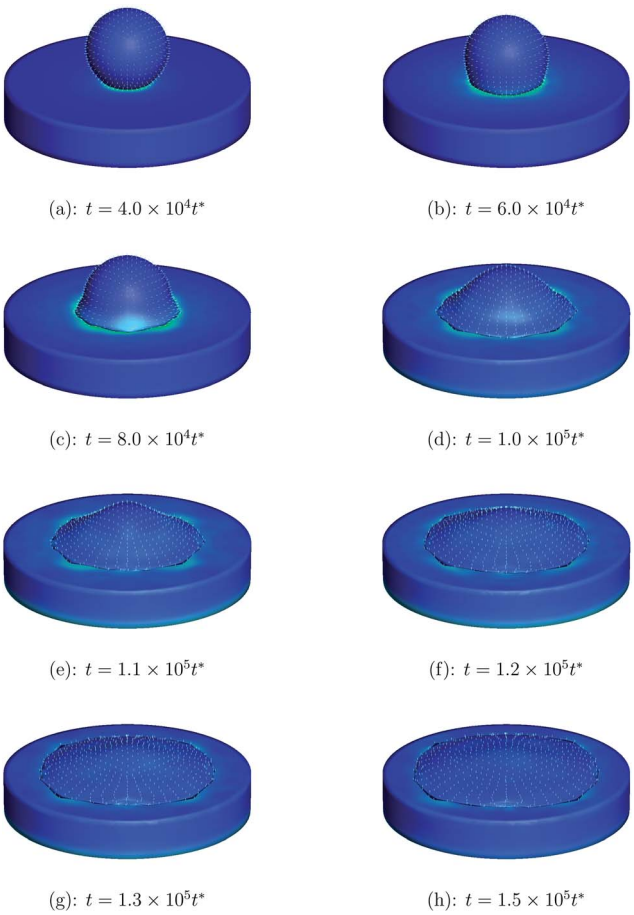

(a): $t = 4.0 \times 10^4 t^*$ (b): $t = 6.0 \times 10^4 t^*$

(c): $t = 8.0 \times 10^4 t^*$ (d): $t = 1.0 \times 10^5 t^*$

(e): $t = 1.1 \times 10^5 t^*$ (f): $t = 1.2 \times 10^5 t^*$

(g): $t = 1.3 \times 10^5 t^*$ (h): $t = 1.5 \times 10^5 t^*$

Fig. 9 Time sequence of cell spreading over Substrate III (stiffness uniform).

motion. In specific, we prescribe the hyperelastic part of the constitutive parameters in the substrate as a function of θ as follows,

$$C_1^S = C_1(2.0 + 8.0\bar{\theta}),\ C_2^S = C_2(2.0 + 8.0\bar{\theta}),\ \lambda^S = \lambda(2.0 + 8.0\bar{\theta})$$

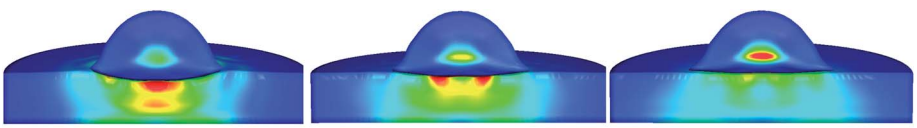

(a) (b) (c)

Fig. 8 Effective Stress over substrates with different stiffness: (a) Substrate-I, (b) Substrate-II, (c) Substrate-III.

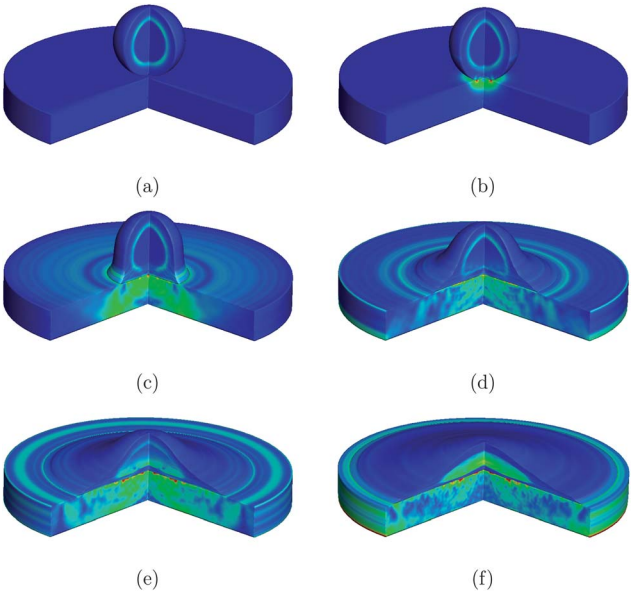

Fig. 10 Time sequence of the cell spreading in axisymmetric simulation.

where $\bar{\theta}$: $= \theta/\pi$ with the center of the substrate at $x = 0$, $y = 0$. The precise problem statement is shown in Fig. 11.

In Fig. 12, we display a time sequence of a cell spreading over the elastic stiffness-varying deformable substrate. For a homogeneous elastic stiffness, a cell would move approximately in the same speed in every radius directions of the substrate, for comparison purpose, in Fig.9, we display a time sequence of a cell spreading in a homogeneous substrate. Based on the simulation results obtained from the inhomogeneous substrates, one may find that the cell actually moves slightly towards the right side ($\theta = \pi$) of the substrate faster than to the left side ($\theta = 0$) of the substrate due to the stiffness gradient. This not only demonstrates a preliminary cell crawling and protrusion behavior, but also indicates that the cell motility is in favor of a stiffer substrate. This results agree with experimental measurements of cell adhesion and migration reported in ref. 5 and 74.

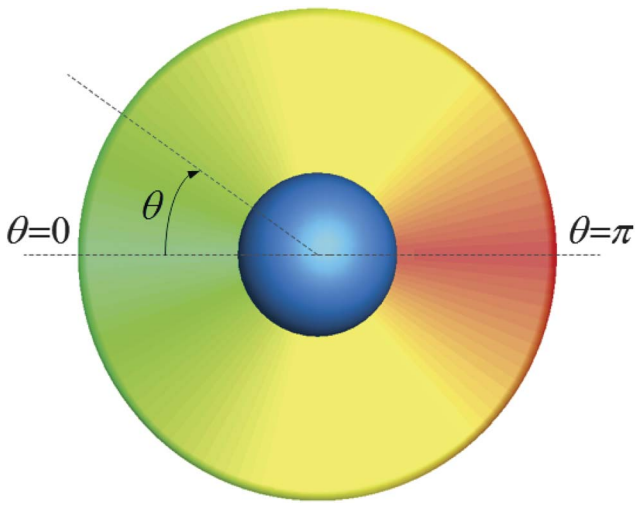

Fig. 11 3D Computational model of cell spreading on a stiffness-varying substrate, the color in the substrate stands for different stiffness, the stiffness at the right end is the highest (top view).

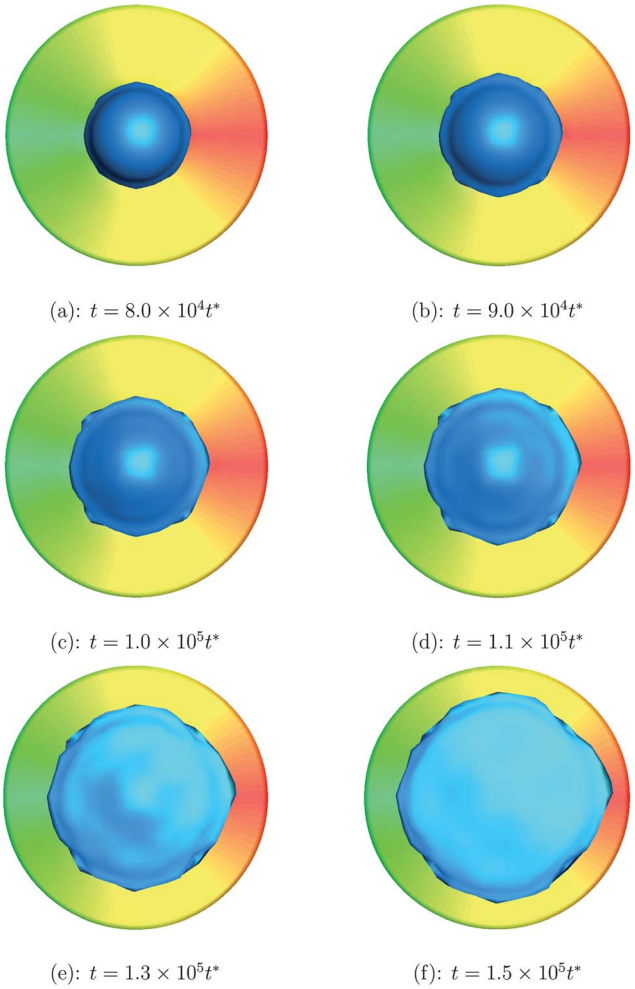

Fig. 12 Time sequence of a 3D cell spreading over a stiffness-varying substrate (top view).

In order to predict cell crawling or mobility, it is crucial to include an active stress in the constitutive modeling of the cell. The active stress term, $-\zeta h_i h_j$, provides contractile force that will generate internal treadmilling of actin cytoskeleton gel. This is because that the term, $-\zeta h_i h_j$, represents the stress contribution from the coupling from dipolar stress. We also believe that at mesoscale level or phenomenological level, the stress contribution term, $\eta h_{k,i} h_{k,j}$, may also affect cell motility, because it is the contribution due to the distortion of director field.

Moreover, recent experimental results have demonstrated that geometrical properties such as cell shape and configuration also play an important role in regulating stem cell lineage, *e.g.* ref. 75. In particular, the experimental results in ref. 76 have shown that the advancing adhesion front of a circular contact zone of a 3D vesicle is unstable under small perturbation. Once reaching a critical value, it easily becomes modulated or wavy. This particular feature of cell spreading can be captured by our soft matter cell model automatically. Fig. 12 reveals a clear picture of the spreading front modulation as the spreading area become large. It may be noted that our previous soft matter cell model and simulation are restricted to 2D plain strain or the axisymmetric case, and it fails to predict the phenomenon of a wavy adhesive front (see ref. 39).

As mentioned in Section 3, two kinds of adhesive forces are used in the simulations. The first is the non-specific long range van der Waals force (see eqn (12)), and the second is the specific ligand–receptor bonding force (see eqn (16)). The parameter values for the specific covenant bond potential are taken from ref. 28 and 79. The value of the parameter D for the van der Waals attractive force in eqn (18) should be proportional to the attractive force between a material particle and a half space, *i.e.* $D \sim A_H/r_0^3$, where A_H is the Hamaker constant.[72] We have chosen r_0 in a range 10 nm $\sim$ 100 nm. Considering $A_H = 10^{-19}$ J, the estimate on D is about correct. However, in eqn (18) we choose d_0 to be two or three orders of magnitude larger than r_0 in order to accelerate the computation.

6. Discussions

Even though the active actomyosin gel model has been studied for almost a decade *e.g.* ref. 61, it is still in its infancy for predicting real cell motion or evolution. To develop a three-dimensional, computational, polarized viscoelastic gel model for cells, that is capable of explaining cell adhesion, locomotion, mechanotransduction, and its structure transformation, is a challenge task, especially if we want it to predict real cellular motion and transformation.

The proposed 3D multiscale and computational soft matter cell model is only the first step towards this goal. In this work, we are mainly concerned with modeling the mechanotransduction of embryonic stem cells, which are still under development. Therefore, the cell model proposed here may not be capable of describing some complex biological functions of functional cells such as stress fiber remodeling. However, we have shown that the present model may be used as a simulation tool to qualitatively study the contact and adhesion of stem cells to gain understanding of the mechanotransduction of stem cells and other issues about cell sensing and signaling.

The simulation results presented in this paper have shown that: (1) By using the proposed soft matter cell model, when a "cell" is in contact with a substrate, its local effective stress level may depend on stiffness of the substrate (see Fig. 8); (2) The size of spreading area of the cell is also depending on the stiffness of extracellular substrate (see Fig. 6); (3) The adhesion front of the cell will become wavy once the spreading radium reaches a certain value (see Fig. 12); and (4) Cell motility is in favor of a stiffer region of a substrate (see Fig. 12).

It should be noted that the behavior of cells, in particular those of stem cells, are complex biological phenomena. The proposed soft matter cell model is only intended to model the mechanical behavior of cells at a mesoscale level, which may not and cannot explain the molecular mechanisms of cellular processes such as evolution and proliferation. To understand the molecular mechanism of the cellular process requires an in-depth study of all aspects of molecular cell biology including all relevant bio-chemical, bio-physical, as well as bio-mechanical factors and their interactions at different scales.

Developing active soft matter models for cells, especially for stem cells, may help us understand the mechano-biology of cells. It has been shown in this work that the soft matter cell model may offer a unique approach that is sound in thermodynamics and statistical bio-mechanics. It provides improved explanations of the interaction between the stem cell and its mechanical niche than those of conventional hyperelastic or viscoelastic cell models. In some cases, the soft matter model has even shown its predictive power, such as cellular morphology change and the origin of cell motility.[39] It is the authors' opinion that by combining the soft matter cell model with molecular simulation we may be able to quantitative simulate and hence predict cellular mechanotransduction process in collaborating with experimental observation. The predictive ability of the soft matter cell model may provide both scientific insight as well as clinic guidance on many of health care problems, such as regenerated medicine and drug design and delivery problems.

The soft matter cell model presented in this work is a primitive one, but it may have open a door for more realistic and more accurate modeling of cells, especially for stem cells. It is possible that more sophisticated soft matter models can be developed along this line by incorporating chemomechanical features at a molecular level that are capable of simulating self-assembly of focal adhesion, cell division, proliferation and more.

Acknowledgements

This research is supported by the A. Richard Newton Research Breakthrough Award from Microsoft Corporation and a grant from National Science Foundation (CMMI No. 0800744). Their support is greatly appreciated. Mr. Houfu Fan and Ms. Yan Zhang have helped to implement several simulation examples at the late stage of this research. The authors would like to thank the two anonymous reviewers who pointed out the importance of the active stress in cell spreading modeling to us.

References

1 M. Liu, Y. Qin, J. Liu, A. K. Tanswell and M. Post, Mechanical strain induces pp60 ^{src} activation and translocation to cytoskeleton in fetal rat lung cells, *J. Biol. Chem.*, 1996, **271**, 7066–7071.
2 O. P. Hamill and B. Martinac, Molecular basis of mechanotransduction in living cells, *Physiol. Rev.*, 2001, **81**, 685–740.
3 K. S. Kolahi and M. R. Mofrad, Mechanotransduction: a major regulator of homeostasis and development, *Wiley Interdiscip. Rev.: Syst. Biol. Med.*, 2010, **2**(6), 625–639.
4 D. E. Discher, P. Janmey and Y. L. Wang, Tissue cells feel and respond to the stiffness of their substrate, *Science*, 2005, **310**, 1139–1143.
5 A. J. Engler, S. Sen, H. L. Sweeney and D. E. Discher, Matrix elasticity directs stem cell lineage specification, *Cell*, 2006, **126**, 677–689.
6 D. Cuvelier, M. Thery, Y. Chiu, S. Dufour, J. Thiery, M. Bornens, P. Nassoy and L. Mahadevan, The universal dynamics of cell spreading, *Curr. Biol.*, 2007, **17**, 694–699.
7 F. Vernerey and M. Farsad, An Eulerian/XFEM formulation for the large deformation of cortical cell membrane, *Comput. Methods Biomech. Biomed. Eng.*, 2011, **14**, 433–445.
8 T. Yeung, P. C. Georges, L. A. Flanagan, B. Marg, M. Ortiz, M. Funaki, N. Zahir, W. Ming, V. Weaver and P. A. Janmey, Effects of substrate stiffness on cell morphology, cytoskeletal structure, and adhesion, *Cell Motil. Cytoskeleton*, 2005, **60**, 24–34.
9 M. J. Paszek, N. Zahir, K. R. Johnson, J. N. Lakins, G. I. Rozenberg, A. Gefen, C. A. Reinhart-King, S. S. Margulies, M. Dembo, D. Boettiger, D. A. Hammer and V. M. Weaver, Tensional homeostasis and the malignant phenotype, *Cancer Cell*, 2005, **8**, 241–254.
10 J. P. Winer, S. Oake and P. A. Janmey, Non-Linear Elasticity of Extracellular Matrices Enables Contractile Cells to Communicate Local Position and Orientation, *PLoS One*, 2009, **4**(7), e6382.

11 J. H.-C. Wang, Substrate deformation determines actin cytoskeleton reorganization: a mathematical modeling and experimental study, *J. Theor. Biol.*, 2000, **202**, 33–41.
12 T. Bickel and R. Bruinsma, Focal adhesion: physics of a biological mechano-sensor, 2003, arXiv:condmat0306116v1.
13 I. L. Novak, B. M. Slepchenko, A. Mogilner and L. M. Loew, Cooperativity between cell contractility and adhesion, *Phys. Rev. Lett.*, 2004, **93**, 268109.
14 T. Shemesh, B. Geiger, A. D. Bershadsky and M. M. Kozlov, Focal adhesions as mechanosensors: a physical mechanism, *Proc. Natl. Acad. Sci. U. S. A.*, 2005, **102**, 12383–12388.
15 R. Bruinsma, Theory of force regulation by nascent adhesion sites, *Biophys. J.*, 2005, **89**, 87–94.
16 A. Bershadsky, M. L. Ran, L. Carramusa, P.-K. Masha, K. Arnold, S. Boguslavsky, E. Landau and Y. Zilberman, Cytoskeleton-adhesion crosstalk: molecular and biophysical aspects, *Life Science Open Day, Weizmann Institute of Science*, 2006.
17 D. R.-B. Aroush and H. D. Wagner, Shear-stress profile along a cell focal adhesion, *Adv. Mater.*, 2006, **18**, 1537–1540.
18 A. Besser and S. A. Safran, Force-induced adsorption and anisotropic growth of focal adhesion, *Biophys. J.*, 2006, **90**, 3469–3484.
19 U. Schwarz, Soft matters in cell adhesion: rigidity sensing on soft elastic substrate, *Soft Matter*, 2007, **3**, 263–266.
20 F. Rehfeldt and D. E. Discher, Cell dipoles feel their way, *Nat. Phys.*, 2007, **3**, 592–593.
21 N. Wang, J. D. Tytell and D. E. Ingber, Mechanotransduction at a distance: mechanically coupling the extracellular matrix with the nucleus, *Nat. Rev. Mol. Cell Biol.*, 2009, **10**, 75–82.
22 M. A. Wozniak and C. Chen, Mechanotransduction in development: a growning role for contractility, *Nat. Rev. Mol. Cell Biol.*, 2009, **10**, 34–43.
23 A. Zemel, F. Rehfeldt, A. E. X. Brown, D. E. Discher and S. A. Safran, Optimal matrix rigidity for stress-fibre polarization in stem cells, *Nat. Phys.*, 2010, **6**, 468–473.
24 F. Vernerey and M. Farsad, A constrained mixture approach to mechano-sensing and force generation in contractile cells, *J. Mech. Behav. Biomed. Mater.*, 2011, **4**(8), 1683–1699.
25 V. S. Deshpande, M. Mrksich, R. M. McMeeking and A. G. Evans, A bio-mechanical model for coupling cell contractility with focal adhesion formation, *J. Mech. Phys. Solids*, 2008, **56**, 1484–1510.
26 P. Liu, Y. W. Zhang, Q. H. Cheng and C. Lu, Simulations of the spreading of a vesicle on a substrate surface mediated by receptor-ligand binding, *J. Mech. Phys. Solids*, 2007, **55**, 1166–1181.
27 L. Sun, Q. H. Cheng, H. J. Gao and Y. W. Zhang, Computational modeling for cell spreading on a substrate mediated by specific interactions, long-range recruiting interactions, and diffusion of binders, *Phys. Rev. E: Stat., Nonlinear, Soft Matter Phys.*, 2009, **79**, 061907.
28 S. Roy and H. Jerry Qi, A computational biomimetic study of cell crawling, *Biomech. Model. Mechanobiol.*, 2010, **9**, 573–581.
29 A. S. Sarvestani and E. Jabbari, Modeling the kinetics of cell membrane spreading on substrates with ligand density gradient, *J. Biomech.*, 2008, **41**, 921–1863.
30 A. S. Sarvestani, A model for cell motility on soft bio-adhesive substrates, *J. Biomech.*, 2011, **44**, 755–758.
31 B. Rubinstein, M. F. Fournier, K. Jacobson, A. B. Verkhovsky and A. Mogilner, actin–myosin viscoelastic flow in the keratocyte lamellipod, *Biophys. J.*, 2009, **97**, 1853–1863.
32 C. M. Coppin and P. C. Leavis, Quantitation of liquid-crystalline ordering in F-actin solutions, *Biophys. J.*, 1992, **63**, 794–807.
33 R. Furukawa, R. Kundra and M. Fechheimer, Formation of liquid crystal from actin filaments, *Biochemistry*, 1993, **32**, 12346–12352.
34 J. Kas, H. Strey, J. X. Tang, D. Finger, R. Ezzell, E. Sachmann and P. A. Janmey, F-actin, a model polymer for semiflexible chains in dilute, semidilute, and liquid crystalline solutions, *Biophys. J.*, 1996, **70**, 609–625.
35 J. Viamonte, S. Narayanan, A. R. Sandy and J. X. Tang, Orientational order parameter of the nematic liquid crystalline phase of F-actin, *Phys. Rev. E: Stat., Nonlinear, Soft Matter Phys.*, 2006, **73**, 061901.
36 J. Viamontes and J. X. Tang, Continuous isotropic-nematic liquid crystalline transition of F-actin solutions, *Phys. Rev. E: Stat. Phys., Plasmas, Fluids, Relat. Interdiscip. Top.*, 2003, **67**, 040701.
37 P. W. Oakes, J. Viamontes and J. Tang, Growth of tactoidal droplets during the first-order isotropic to nematic phase transition of F-actin, *Phys. Rev. E: Stat., Nonlinear, Soft Matter Phys.*, 2007, **75**, 069102.
38 J. He, M. Mak, Y. Liu and J. X. Tang, Counterion-dependent microrheological properties of F-actin solutions across the isotropic-nematic phase transition, *Phys. Rev. E: Stat., Nonlinear, Soft Matter Phys.*, 2008, **78**, 011908.
39 X. Zeng and S. Li, Multiscale modeling and simulation of soft adhesion and contact of stem cells, *J. Mech. Behav. Biomed. Mater.*, 2011, **4**, 180–189.
40 S. J. Singer and G. L. Nicolson, The fluid mosaic model of the structure of cell membranes, *Science*, 1972, **175**, 720–731.
41 W. Helfrich, Elastic properties of lipid bilayer: theory and possible experiments, *Z. Naturforsch., C: J. Biosci.*, 1973, **28**, 693–703.
42 J. P. McGarry, B. P. Murphy and P. E. McHugh, Computational mechanics modeling of cell-substrate contact during cyclic substrate deformation, *J. Mech. Phys. Solids*, 2005, **53**, 2597–2637.
43 H. Karcher, J. Lammerding, H. Huang, R. T. Lee, R. D. Kamm and M. R. K. Mofrad, A three-dimensional viscoelastic model for cell deformation with experimental verification, *Biophys. J.*, 2003, **85**, 3336–3349.
44 N. Wang, J. P. Butler and D. E. Ingber, Mechanotransduction across the cell surface and through the cytoskeleton, *Science*, 1993, **260**, 1124–1127.
45 D. E. Ingber, Tensegrity: the architectural basis of cellular mechanotransduction, *Annu. Rev. Physiol.*, 1997, **59**, 575–599.
46 A. E. Carlsson, Contractile stress generation by actomyosin gels, *Phys. Rev. E: Stat., Nonlinear, Soft Matter Phys.*, 2006, **74**, 051912.
47 F. Chowdhury, S. Na, D. Li, Y. Poh, T. S. Tanaka, F. Wang and N. Wang, Material properties of the cell dictate stress-induced spreading and differentiation in embryonic stem cells, *Nat. Mater.*, 2010, **9**, 82–88.
48 S. J. Woltman, G. D. Jay and G. P. Crawford, Liquid-crystal materials find a new order in biomedical applications, *Nat. Mater.*, 2007, **6**, 929–938.
49 F. H. Lin and C. Liu, Existence of solutions for the Ericksen-Leslie system, *Arch. Ration. Mech. Anal.*, 2000, **154**, 135–156.
50 N. Caille, O. Thoumine, Y. Tardy and J. Meister, Contribution of the nucleus to the mechanical properties of endothelial cells, *J. Biomech.*, 2002, **35**, 177–187.
51 A. J. Maniotis, C. S. Chen and D. E. Ingber, Demonstration of mechanical connections between integrins, cytoskeletal filaments, and nucleoplasm that stabilize nuclear structure, *Proc. Natl. Acad. Sci. U. S. A.*, 1997, **94**, 849–854.
52 G. Marckmann and E. Verron, Comparison of hyperelastic models for rubberlike materials, *Rubber Chem. Technol.*, 2006, **79**(5), 835–858.
53 I. Fried and A. R. Johnson, A note on elastic energy density functions for largely deformed compressible rubber solids, *Comput. Methods Appl. Mech. Eng.*, 1988, **69**, 53–64.
54 S. Sen, A. J. Engler and D. E. Discher, Matrix strains induced by cells: computing how far cells can feel, *Cell. Mol. Bioeng.*, 2009, **2**, 39–48.
55 S. Fereol, R. Fodil, V. M. Laurent, M. Balland, B. Louis, G. Pelle, S. Hnon, E. Planus and D. Isabey, Prestress and adhesion site dynamics control cell sensitivity to extracellular stiffness, *Biophys. J.*, 2009, **96**, 2009–2022.
56 K. Kruse, J. F. Joanny, F. Jülicher, J. Prost and K. Sekimoto, Asters, vortices, and rotating spirals in active gels of polar filaments, *Phys. Rev. Lett.*, 2004, **92**, 078101.
57 K. Kruse, J. F. Joanny, F. Jülicher, J. Prost and K. Sekimoto, Generic theory of active polar gels: a paradigm for cytoskeletal dynamics, *Eur. Phys. J. E*, 2005, **16**, 5–16.
58 K. Kruse, J. F. Joanny, F. Jülicher and J. Prost, Contractility and retrograde flow in lamellipodium motion, *Phys. Biol.*, 2006, **3**, 130–137.
59 J. F. Joanny and J. Prost, Active gels as a description of the actin–myosin cytoskeleton, *HFSP J.*, 2009, **3**, 94–104.
60 F. Jülicher, K. Kruse, J. Prost and J. F. Joanny, Active behavior of the Cytoskeleton, *Phys. Rep.*, 2007, **449**, 3–28.
61 R. A. Simha and S. Ramaswamy, Hydrodynamic fluctuations and instabilitiesin ordered suspensions of self-propelled particles, *Phys. Rev. Lett.*, 2002, **89**, 058101.
62 S. Ramaswamy and M. Rao, Active-filament hydrodynamics: instabilities, boundary conditions and rhelogy, *New J. Phys.*, 2007, **9**(423), 1–9.

63 M. E. Cates, S. M. Fielding, D. Marenduzzo, E. Orlandini and J. M. Yeomans, Shearing active gels close to the isotropic-nematic transition, *Phys. Rev. Lett.*, 2008, **101**, 068102.
64 S. A. Edwards and J. M. Yeomans, Spontaneous flow states in active nematics: A unified picture, *Europhys. Lett.*, 2009, **85**, 18008.
65 L. M. Yang, V. P. W. Shim and C. T. Lim, A visco-hyperelastoc approach to modelling the constitive behaviour of rubber, *Int. J. Impact Eng.*, 2000, **24**, 545–560.
66 L. M. Yang and V. P. W. Shim, A visco-hyperelastic constitutive description of elastomeric foam, *Int. J. Impact Eng.*, 2004, **30**, 1099–1110.
67 S. Li and W. Kam Liu, *Meshfree Particle Methods*, Springer, Berlin, 2004.
68 R. Sauer and S. Li, A contact mechanics model for quasi-continua, *Int. J. Numer. Methods Eng.*, 2007, **71**, 931–962.
69 T. Belytschko, W. K. Liu and B. Moran, *Nonlinear Finite Elenments for Continua and Structures*, Wiley, 2000.
70 X. Zeng and S. Li, Modeling and simulation of substrate elasticity sensing in stem cells, *Comput. Methods Biomech. Biomed. Eng.*, 2011, **14**, 447–458.
71 G. A. Holzapfel, *Nonlinear Solid Mechanics: A Continuum Approach for Engineering* Wiley, 2000.
72 J. N. Israelachvili, *Intermolecular and surface forces*, Academic Press, 3rd edn, 2010.
73 Y. Ni and M. Chiang, Cell morphology and migration linked to substrate rigidity, *Soft Matter*, 2007, **3**, 1285–1292.
74 J. Y. Wong, A. Velasco, P. Rajagopalan and Q. Pham, Directed movement of vascular smooth muscle cells on gradient-compliant hydrogels, *Langmuir*, 2003, **19**, 1908–1913.
75 R. McBeath, D. M. Pirone, C. M. Nelson, K. Bhadriraju and C. S. Chen, Cell shape, cytoskeleton tension, and RohA regulate stem cell lineage commitment, *Dev. Cell*, 2004, **6**, 483–495.
76 A. Boulbitch, Z. Guttenberg and E. Sackmann, Kinetics of membrane adhesion mediated by ligand–receptor interaction studied with a biomimetic system, *Biophys. J.*, 2001, **81**, 2743–2751.
77 G. I. Bell, Models for the specific adhesion of cells to cells, *Science*, 1978, **200**, 618–627.
78 G. I. Bell, M. Dembo and P. Bongrand, Cell adhesion: competition between nonspecific repulsion and specific bonding, *Biophys. J.*, 1984, **45**, 1051–1064.
79 U. Seifert, Adhesion of vesicles in two dimensions, *Phys. Rev. A: At., Mol., Opt. Phys.*, 1991, **43**, 6803–6814.

